Ono, T., Sinclair, G., Bonneau, D., Thompson, M., Matthews, J., & Rarity, J. (2019). Observation of nonlinear interference on a silicon photonic chip. *Optics Letters*, *44*(5), 1277-1280. https://doi.org/10.1364/OL.44.001277

Observation of non-linear interference on a silicon photonic chip

TAKAFUMI ONO[1*], GARY F. SINCLAIR[1], DAMIEN BONNEAU[1], MARK G. THOMPSON[1], JONATHAN C. F. MATTHEWS[1], AND JOHN G. RARITY[1]

[1] *Quantum Engineering Technology Labs, H. H. Wills Physics Laboratory and Department of Electrical & Electronic Engineering, University of Bristol, BS8 1FD, UK.*

[*] *Corresponding author: Takafumi.Ono@bristol.ac.uk*

Compiled February 6, 2019

Photonic integrated circuits represent a promising platform for applying quantum information science to areas such as quantum computation, quantum communication and quantum metrology. While the linear optical approach has greatly contributed to this field, it is often possible to improve the functionality and scalability by making use of non-linear processes. One interesting process is the interference between two non-linear optical processes, where the interference occurs by removing the information as to which of two processes have occurred. In this Letter, we demonstrate a non-linear interferometer in the pair-photon generation regime by using spontaneous four-wave mixing in an integrated silicon photonic chip. We observe a non-linear interference in the production rate of photon pairs generated from two different four-wave mixing waveguides. We obtain an interference visibility of 96.8%. This work shows the possibility of integrating and controlling nonlinear-optical interference components for silicon quantum photonics.

OCIS codes: (120.3180) Interferometry; (130.3120) Integrated optics devices; (230.7370) Waveguides; (250.5300) Photonic integrated circuits; (270.0270) Quantum optics; (270.5585) Quantum information and processing

http://dx.doi.org/10.1364/ao.XX.XXXXXX

Photonic integrated circuits are a promising platform for realizing large-scale photonic devices. Silicon photonics, in particular, is a leading platform because of the component density, mature fabrication processing, and compatibility with both telecom optics and CMOS electronics [1]. Silicon photonics is also considered a promising physical implementation for quantum information technologies, including quantum photonic circuits, on-chip spontaneous photon-pair generation [2, 3], multi-port electro-optic switching [4] and on-chip detection of a quantum state of light [5–7]. These developments open up new possibilities in integrated quantum technology such as large scale quantum computation [9, 10], quantum communication [11], quantum machine-learning [12] and quantum-enhanced sensing [13, 14]. In principle, any quantum information task can be realized by using a linear optical circuit which combines probabilistic two-qubit gates [15, 16] and single qubit operations [17]. However, it has been proposed that nonlinear effects could be used to improve the functionality and scalability of such circuits [18]. One such interesting effect is the interference between two non-linear optical processes, where the interference occurs by deleting the "which-source" information[19–22], referred to as nonlinear interferometry [23, 24].

Nonlinear interferometers were originally considered by Yurke to improve a measurement sensitivity where the signal is amplified via parametric amplification while keeping its noise level close to the vacuum noise level [25, 26]. Later, a similar configuration but in the lower photon number regime was considered and experimentally demonstrated, where photon pairs were used to observe the interference [27]. In contrast to a conventional Mach-Zehnder interferometer, in a nonlinear interferometer the two beam splitters are replaced by two nonlinear elements where both elements are pumped by the laser to create signal and idler photons [27]. The creation probability of generating the photon pairs at the second element is determined by a total phase of the signal, idler and pump fields, so that the intensity of the photon pairs after the second element is sensitive to a change in the phase of any one of the three fields [19, 27]. Several proposals have been made, and demonstrations performed, that use this effect in bulk optics. These include quantum imaging at one wavelength without detecting photons at that wavelength [28], infrared spectroscopy by detecting correlated visible photons [29] and several methods of creating useful quantum states [30]. It is also interesting and important to establish this type of technology in integrated quantum photonics, which provides unrivalled scale, control and manufacturability of complex quantum photonic systems.

Here we demonstrate a non-linear interferometer using spontaneous four-wave mixing (SFWM) in a χ^3 nonlinear integrated silicon photonic chip. We produce a photon pair by SFWM, where signal and idler photons propagate together in single mode waveguide. A high quality of spatial mode matching among signal, idler and pump fields results in high visibility interference of more than 96 %. We also confirm the dependence of the interference visibility on the ratio of the two amplitudes

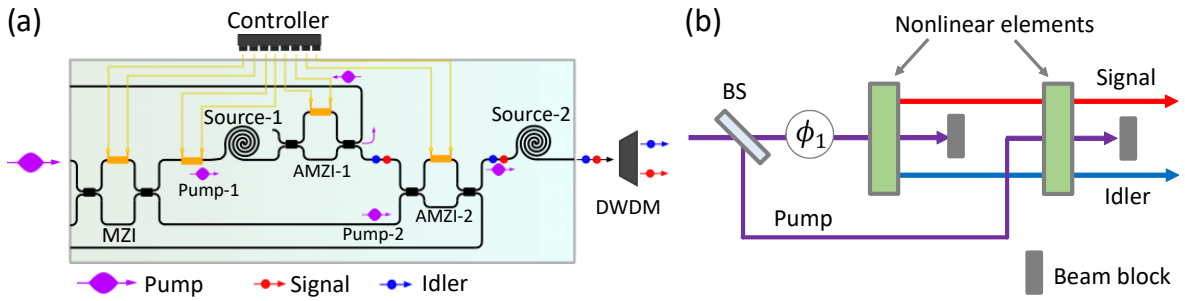

Fig. 1. Experimental set-up. (a) Design of a non-linear interferometer on a silicon photonic chip. Generation of signal and idler photons occurs in the first spiraled waveguide source (Source-1) and is enhanced/suppressed in the second spiraled waveguide source (Source-2) on a silicon photonic chip. The chip was fixed on a copper PCB and its temperature are controlled and stabilized by using temperature controller (Thorlab TED200C). Phases of each interferometer were adjusted by thermal phase shifters. (b) Illustration of the concept. BS: Beam splitter. AMZI: Anti-symmetric Mach-Zehnder interferometer.

of the photon pairs, which is consistent with our theoretical prediction. We believe this experimental demonstration shows the possibility of integrating and controlling nonlinear-optical components for silicon quantum photonics.

Figure 1 (a) illustrates our integrated non-linear interferometer composed of two spiraled waveguides, one Mach-Zehnder Interferometer (MZI) and two anti-symmetric MZIs (AMZIs). The corresponding setup in a bulk optics implementation is shown in figure 1(b) and is typical of the principle of non-linear interferometry in the low gain regime. A continuous-wave pump field is split coherently into two paths by using an MZI configured to act as a 50:50 beam splitter. One beam (Pump-1) is directed to spiraled waveguide (Source-1) and the other beam (Pump-2) is directed to the other spiraled waveguide (Source-2). Generation of signal and idler photons first occurs in Source-1 by SFWM. The interaction Hamiltonian $\hat{H}$ is expressed in terms of the three fields of the pump (A_p), signal (s) and idler (i) as $\hat{H} \propto A_p^2 \hat{a}_s^\dagger \hat{a}_i^\dagger + (A_p^*)^2 \hat{a}_s \hat{a}_i$, where $\hat{a}$ and $\hat{a}^\dagger$ are annihilation and creation operators. When the pair probability is sufficiently small, the quantum state produced can be approximated by,

$$|\psi_1\rangle \approx |0\rangle_s |0\rangle_i + \alpha_1 |1\rangle_s |1\rangle_i, \quad \textbf{(1)}$$

where $\alpha_1 \propto A_{p1}^2$ results in a magnitude of the complex amplitude $\alpha_1 = |\alpha_1| e^{i\phi_1}$ that depends on pump power and a phase that depends on the phases of Pump-1 (ϕ_{p1}), signal (ϕ_{s1}) and idler (ϕ_{i1}) of the input fields as given by $\phi_1 = 2\phi_{p1} - \phi_{s1} - \phi_{i1}$. Here, we neglect the effects of self- and cross-phase modulation, which will be insignificant in the low-power pump regime used. In addition, phase factors due to phase-matching of the source are also not explicitly stated, as these will result in an unimportant constant phase offset of the state in our experiment.

After Source-1, Pump-1 is filtered out by using AMZI-1. The signal and idler photons ($|\ 1\rangle_s\ |\ 1\rangle_i$) are then combined with Pump-2 using AMZI-2 which has the same structure as AMZI-1 (but operating in reverse). Signal and idler photons along with Pump-2 then pass to the second spiral source (Source-2).

After Source-2, the quantum state is a superposition of two states where one is expressed by eq.(1) and the other is expressed by the same formula as eq.(1) but with a different amplitude of $\alpha_2 = |\alpha_2| e^{i\phi_2}$, where the phase of ϕ_2 depends on the phases of Pump-2 (ϕ_{p2}), signal (ϕ_{s2}) and idler (ϕ_{i2}) of the input modes as given by $\phi_2 = 2\phi_{p2} - \phi_{s2} - \phi_{i2}$. The post-selected output state $|\psi\rangle$ of the two fold coincidence is then given by

$$|\psi\rangle \propto \alpha_1 |1\rangle_s |1\rangle_i + \alpha_2 |1\rangle_s |1\rangle_i = (\alpha_1 + \alpha_2)\, |1\rangle_s |1\rangle_i. \quad \textbf{(2)}$$

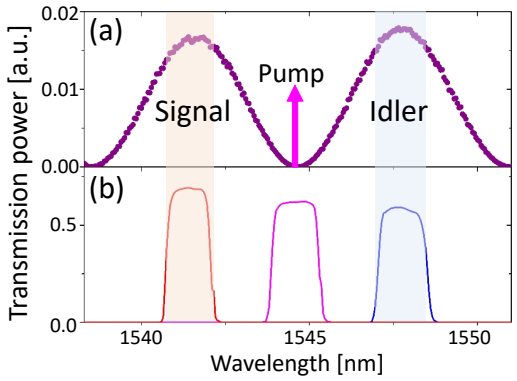

Fig. 2. (a) Dependence of output power of AMZIs on phase. Free spectral range of the AMZIs are 3.2 nm. (b) Transmission spectrum of off-chip DWDM.

The probability that two photons are detected after Source-2 is proportional to the square of the absolute value of the coefficients of the equation (2), which is expressed as $P(\phi) \propto |\alpha_1 + \alpha_2|^2 = |\alpha_1|^2 + |\alpha_2|^2 + 2|\alpha_1||\alpha_2| \cos(\phi)$, where $\phi = \phi_1 - \phi_2$ is the relative phase between the coefficients α_1 and α_2. Thus the interference between two non-linear processes is observed in the production rate of the photons pairs at the output by changing the relative phase ϕ. In the experiment, we varied the phase of Pump-1 ϕ_{p1} (see fig. 1), so that the relative phase ϕ is a function of ϕ_{p1} as given by $\phi = 2\phi_{p1} + \Phi_0$, where $\Phi_0 = -\phi_{s1} - \phi_{i1} - (2\phi_{p2} - \phi_{s2} - \phi_{i2})$ is a constant value.

The normalized interference fringe $f(\phi_{p1})$ for two-photon coincidences can be expressed as,

$$f(\phi_{p1}) = \frac{1}{2}\left(1 + V(R)\cos(2\phi_{p1} + \Phi_0)\right), \quad \textbf{(3)}$$

where $V(R) = 2R/(1+R^2)$ and R is the ratio of the photon-pair state amplitudes such that $R = |\alpha_2|/|\alpha_1|$. The maximum ideal visibility is 1 at $R = 1$ where the production rate of a photon pairs in the first and second sources are equal. Visibility of the interference fringe decreases as the ratio of the production rates between sources 1 and 2 vary from unity.

Our device was fabricated on a standard Silicon-on-Insulator wafer using photo-lithography technology through the IME multi project wafer service. The beamsplitters use a multi-mode

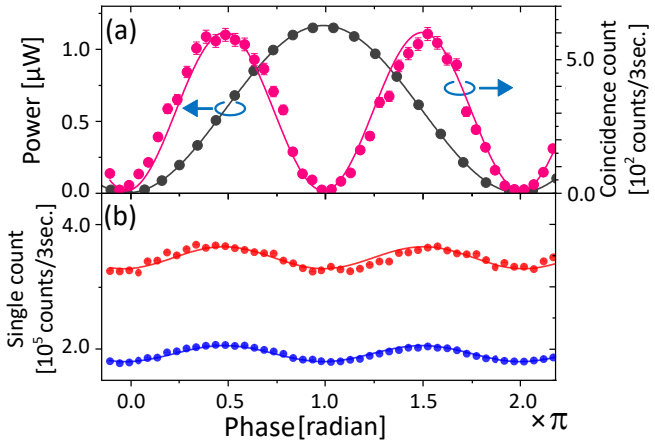

Fig. 3. (a) Interference fringes for classical light and quantum state. Grey data and left vertical axis is the fringe obtained by using standard MZI with classical laser light. Pink data and right axis is the fringe of coincidence counts obtained by using nonlinear interferometer. Here, data collection took three seconds per point. Phase was changed in intervals of $\pi/20$. (b) Interference fringe of single counts. Red and blue are fringes of signal and idler photons, respectively.

interference (MMI) structure and thermo-optical phase-shifters were implemented using resistive heaters. Filters use an asymmetric MZI where the path length difference between each arm is 95 µm, which separates the pump and signal/idler beams. Figure 2(a) shows the transmission spectrum for the AMZI filter, which has a free spectral range about 3.2 nm. The extinction ratio of this filter was about 30 dB. The chip was mounted on a thermo-electrically controlled copper plate to stabilize temperature, with waste heat dissipated by a large copper heat sink. Each phase-shifter has a separate signal pin and mutually referenced ground pin, and was controlled by an custom-made voltage driver. Thermal crosstalk was negligible, and the device remained in a steady thermal state throughout, controlled by a temperature controller with a nominal stability of 0.002 K.

We coupled 10 mW of laser light at 1544.6 nm wavelength from a continuous wave Tunics T100S-HP laser into the chip using grating couplers and a single-mode fiber array mounted on a piezo-controlled 6-axis translation stage. Coupling loss from the fiber to the waveguide was estimated to be 3 dB, indicating power inside the waveguide was 5 mW. Laser light was then divided into two paths which are directed to two spiraled waveguide photon pair sources [2] by using a MZI which acts as tunable beam splitter. The length of the spiraled waveguide was 1.4 cm and the typical coincidence count rate from each spiraled waveguide was 100 counts per second. Produced signal and idler photons are coupled into the fiber through grating couplers and are divided into two optical fibers by using a dense-wavelength-division multiplexer (DWDM) (Figure2 (b)). Non-adjacent crosstalk of our DWDM was 35 dB. Each signal and idler photon is delivered into two off-chip superconducting nano-wire single photon detectors to measure the count rates.

We first discuss linear interference between Pump-1 and Pump-2. Since our non-linear interference relies on the phase difference between two pump fields, the phase relation between Pump-1 and Pump-2 should be well preserved and the two optical modes should be perfectly matched. In this configuration, the phases of MZI and AMZI-2 are adjusted to $\pi/2$ so that input beams are equally split into two output ports, that is, they act as a 50:50 beamsplitter. Also the phase of AMZI-1 is adjusted to 0 so that all of the input beam is delivered to AMZI-2. Figure 3 shows the observed interference fringe by varying ϕ_{p1}. Visibility of the classical interference fringe is 99.5 % which guarantees the coherence between Pump-1 and Pump-2 and the spatial mode matching between two beams.

Figure 3 (a) shows the coincidence counts of signal and idler photons by varying ϕ_{p1}. Figure 3(a) clearly shows that the generation rate of the signal and idler photons at the second spiraled source increases or decreases depending on the phase ϕ_{p1}. The doubled fringe frequency compared with the interference fringe between Pump-1 and Pump-2 indicates that interference occurred between the probability amplitudes for pairs to be produced in Source-1 (from Pump-1) and in Source-2 (from Pump-2). Visibility of the interference fringe was 96.8 ± 2.0 %. Figure 3 (b) shows single counts of signal and idler photons. As expected, the single photon count rate of each signal and idler photon also varies depending on ϕ_1 with the same period of the fringe obtained from coincidence counts. Visibilities of signal and idler photons are 6.6 % and 5.0 %, respectively.

Although the obtained visibility in coincidence counts was reasonably high, we propose that the visibility did not reach unity mainly because of temperature fluctuation (ΔT) of the chip, which causes a change in the refractive index (Δn) of the silicon due to the thermo-optic effect. This is given by $\Delta n = \kappa \Delta T$, where $\kappa = 1.86 \times 10^{-4} \mathrm{K}^{-1}$ [32]. This change causes a phase instability ($\Delta\phi$) between signal and idler photons and pump beam which arrive at the spiraled Source-2 as given by $\Delta\phi = 2\pi \Delta L \Delta n(\Delta T)/\lambda$ where ΔL is the path length difference between two arms of the interferometer and and λ is a wavelength of the light. To include the effect of the phase instability, we assume that the phase drift is distributed around the center of the nominal value of ϕ_0 with a Gaussian distribution as given by $g(\phi - \phi_0) = \mathrm{e}^{-(\phi-\phi_0)^2/2\Delta\phi}/\sqrt{2\pi\Delta\phi}$. The observed interference fringe, $f'(\phi_0)$, is then modeled by the convolution of the eq. (3) and $g(\phi - \phi_0)$,

$$f'(\phi_0) = \int_{-\infty}^{\infty} f(\phi) g(\phi - \phi_0) d\phi = \left(1 + V'(R)\cos(\phi_0)\right)/2, \quad \textbf{(4)}$$

where

$$V'(R) = \mathrm{e}^{-2\Delta\phi} V(R) = \mathrm{e}^{-2\Delta\phi} \frac{2R}{1+R^2}. \quad \textbf{(5)}$$

In our experiment, R was adjusted by changing the relative power used to pump Sources-1 and 2. To characterize the brightness of each source independently, we performed the following procedure. Firstly, using the on-chip MZI all of the pump power was directed towards Source-1 and AMZI-1 was used to remove the pump directly after the source: this ensured that photons were only generated in the Source-1. By adjusting the pump power used the photon-pair generation rate of Source 1 could be measured. Secondly, the on-chip MZI was adjusted to direct all of the pump power to the Source-2. A scan of the pump was again performed to characterize the photon-pair generation rate as a function of the pump power used. In this way, the experimentally measured ratio of the photon-pair generation rates (R), could be related to the pump power employed in each source in subsequent experiments.

Figure 4 shows the visibilities of the two photon interference fringe depending on the ratio of photon pairs generated from Source-1 and Source-2. As expected from eq.(5), visibility of the interference fringe varies depending on the ratio. From

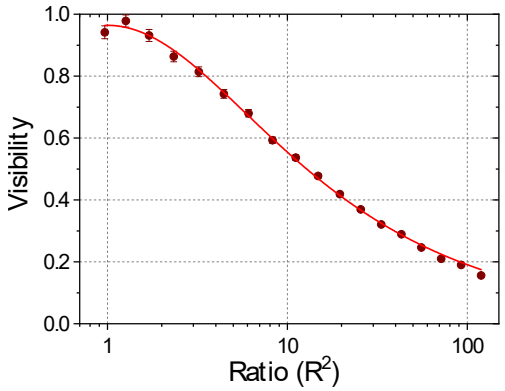

Fig. 4. Dependence of visibility on the ratio of the amplitude of photon pairs produced by first spiraled source and second spiraled source. Visibility was calculated from the experimental data similar to Fig. 3 taken for different ratio of R. Total of 13 mW laser power was used for this measurement, which was split between Source-1 and Source-2 using the on-chip MZI.

the fitting, $\Delta\phi$ was estimated as 0.016 which corresponds the temperature fluctuation of $\Delta T = 0.0014^\circ$ which is consistent of the precision with our temperature controller. We note that the nonlinear interference visibility is more susceptible to fluctuations in path length than the classical measurement using the pump fields. This is due to the fringe period being half that of the classical experiment, resulting in greater sensitivity, and the longer integration time over which the measurements are taken. We also note that the optimal fringe visibility was actually measured at R=1.12, which was likely due to a small error when independently calibrating the brightness of both sources at different pump levels.

We have experimentally demonstrated a nonlinear interferometer on a silicon photonic chip and successfully observed nonlinear interference with a visibility of 96.8 % in coincidence measurements, which is sufficiently high for the application to various quantum tasks [28–30]. We note the low visibility of the signal and idler fringes can be attributed to loss present between the both sources, which has been shown to degrade the single-photon fringe visibility [31]. Assuming an intermediate loss between both lossless sources, the obtained single-photon fringe visibility for the signal and idler photons is consistent with a loss of 14.7 dB and 15.9 dB respectively. This corresponds well to the expected waveguide losses present in each source ($\sim$ 9 dB from two 2.8 cm spiralled sources of typically 3 dB cm^{-1} loss) and of the two AMZI filters ($\sim$ 3 dB each). The slight asymmetry of the losses for the signal and idler photons is likely due to imperfections in the passband or alignment of the on-chip AMZI filters. We have also confirmed the dependence of interference visibility on the ratio of two amplitudes of photon pairs. The measured visibilities were consistent with our theoretical prediction, indicating we understand the factors that currently limit the interference visibility.

In general, our result confirms that integrated silicon photonics can be used in nonlinear interferometry applications that are on-chip. Recent progress in integrated silicon photonics has shown the potential of large-scale quantum architectures, to which nonlinear interferometers have the potential to become a useful additional building block. Also since our device can manipulate the creation of photon pairs by changing the phase of the pump field without accessing signal and idler photons, this device design may be used for optical switching and modulating of FWM photon sources. We expect that the demonstration of an on-chip nonlinear interferometer is a step towards improved functionality and opens new possibilities for silicon quantum photonics.

FUNDING

This work was supported by EPSRC, ERC, PICQUE, BBOI, US Army Research Office (ARO) Grant No. W911NF-14-1-0133, U.S. Air Force Office of Scientific Research (AFOSR) and the Centre for Nanoscience and Quantum Information (NSQI). J.C.F.M. acknowledge fellowship support from the Engineering and Physical Sciences Research Council (EPSRC, UK).

REFERENCES

1. D. Thomson *et al.* J. Opt. **18** 073003 (2016)
2. J. W. Silverstone *et al.* Nat. Photon. **8**, 104-108 (2014).
3. I. E. Zadeh *et al.* Nano Lett. **16** (4) 2289-2294 (2016)
4. L. Qiao, W. Tang & T. Chu Sci. Rep. **7** 42306 (2017)
5. X. Yang, H. Li, W. Zhang, L. You, L. Zhang, X. Liu, Z. Wang, W. Peng, X. Xie, & M. Jiang Opt. Express **22**, 16267-16272 (2014)
6. F. Najafi *et al.* Nat. Commun. **6**, 5873 (2015).
7. F. Raffaelli *et al.* Quantum Sci. Technol. **3**, 025003 (2018).
8. N. C. Harris *et al.* Nanophotonics **5** (3) 456-468 (2016)
9. Harris, N. C. et al. Bosonic transport simulations in a large-scale programmable nanophotonic processor. Preprint at http://arXiv.org/abs/1507.03406 (2015).
10. J. Wang *et al.* 10.1126/science.aar7053 (2018)
11. P. Sibson *et al.* Nat. Commn. **8**, 13984 (2016).
12. J. Wang *et al.* Nat. Phys. **13**, 551–555 (2017).
13. A. Crespi *et al.* Appl. Phys. Lett. **100**, 233704 (2012).
14. M. A. Ciampini *et al.* Sci. Rep. **6**, 28881 (2016).
15. J. L. O'Brien, G. J. Pryde, A. G. White, T. C. Ralph, & D. Branning, Nature **426**, 264–267 (2003).
16. J. Zeuner *et al.* npj Quantum Informationvolume **4**, 13 (2018)
17. M. A. Nielsen and I. L. Chuang Quantum Computation and Quantum Information, Cambridge Series on Information and the Natural Sciences (Cambridge Univ. Press, 2000)
18. X. Qiang *et al.* Nat. Photon. **12**, 534-539 (2018)
19. X. Y. Zou, L. J. Wang, & L. Mandel, Phys. Rev. Lett. **67**, 318–321 (1991).
20. T. J. Herzog, P. G. Kwiat, H. Weinfurter, A. Zeilinger, W. Huang, Phys. Rev. Lett. **75**, 3034–632 (1995).
21. A. Heuer, R. Menzel, and P. W. Milonni Phys. Rev. Lett. **114**, 053601 (2015).
22. A. Heuer, R. Menzel, and P. W. Milonni Phys. Rev. A **92**, 033834 (2015).
23. J. Jing, C. Liu, Z. Zhou, Z. Y. Ou, & W. Zhang Appl. Phys. Lett. **99**, 011110 (2011)
24. Z. Y. Ou Phys. Rev. A **85**, 023815 (2012)
25. B. Yurke, S. L. McCall, and J. R. Klauder Phys. Rev. A **33**, 4033 (1986)
26. F. Hudelist, J. Kong, C. Liu, J. Jing, Z. Y. Ou and W. Zhang Nat. Communs. **5**, 3049 (2014)
27. T. J. Herzog, J. G. Rarity, H. Weinfurter and A. Zeilinger Phys. Rev. Lett. **72**, 629 (1994).
28. G. B. Lemos *et al.* Nature (London) **512**, 409 (2014).
29. D. A. Kalashnikov, A. V. Paterova, S. P. Kulik & L. A. Krivitsky Nat. Photon. **10**, 98-101 (2016)
30. M. Krenn, A. Hochrainer, M. Lahiri, and A. Zeilinger Phys. Rev. Lett. **118**, 080401 (2017).
31. R. Z. Vered, Y. Shaked, Y. Ben Or, M. Rosenbluh & A. Peer Phys. Rev. Lett. **114**, 063902-632 (2015).
32. Q. Xu and M. Lipson Opt. Lett. **31**, 341-343 (2006).
33. Out data are available for download from the Research Data Repository of University of Bristol at doi:tbc.

SECOND REFERENCE LIST

[1] D. Thomson *et al.*, *"Roadmap on silicon photonics"*, J. Opt. **18** 073003 (2016)

[2] J. W. Silverstone *et al.*, *"On-chip quantum interference between silicon photon-pair sources"*, Nat. Photon. **8**, 104-108 (2014).

[3] I. E. Zadeh *et al.*, *"Deterministic Integration of Single Photon Sources in Silicon Based Photonic Circuits"*, Nano Lett. **16** (4) 2289-2294 (2016)

[4] L. Qiao, W. Tang & T. Chu, *"32x32 silicon electro-optic switch with built-in monitors and balanced-status units"*, Sci. Rep. **7** 42306 (2017)

[5] X. Yang, H. Li, W. Zhang, L. You, L. Zhang, X. Liu, Z. Wang, W. Peng, X. Xie, & M. Jiang, *"Superconducting nanowire single photon detector with on-chip bandpass filter"*, Opt. Express **22**, 16267-16272 (2014)

[6] F. Najafi *et al.*, *"On-chip detection of non-classical light by scalable integration of single-photon detectors"*, Nat. Commun. **6**, 5873 (2015).

[7] F. Raffaelli *et al.*, *A homodyne detector integrated onto a photonic chip for measuring quantum states and generating random numbers*, Quantum Sci. Technol. **3**, 025003 (2018).

[8] N. C. Harris *et al.*, *"Large-scale quantum photonic circuits in silicon"*, Nanophotonics **5** (3) 456-468 (2016)

[9] Harris, N. C. et al., *"Bosonic transport simulations in a large-scale programmable nanophotonic processor"*, Preprint at http://arXiv.org/abs/1507.03406 (2015).

[10] J. Wang *et al.*, *"Multidimensional quantum entanglement with large-scale integrated optics"*, 10.1126/science.aar7053 (2018)

[11] P. Sibson *et al.*, *"Chip-based quantum key distribution"*, Nat. Commn. **8**, 13984 (2016).

[12]J. Wang *et al.*, *"Experimental quantum Hamiltonian learning"*, Nat. Phys. **13**, 551-555 (2017).

[13] A. Crespi *et al.*, *"Measuring protein concentration with entangled photons"*, Appl. Phys. Lett. **100**, 233704 (2012).

[14] M. A. Ciampini *et al.*, *"Quantum-enhanced multiparameter estimation in multiarm interferometers"*, Sci. Rep. **6**, 28881 (2016).

[15] J. L. O'Brien, G. J. Pryde, A. G. White, T. C. Ralph, & D. Branning,, *"Demonstration of an all-optical quantum controlled-NOT gate"*, Nature **426**, 264–267 (2003).

[16] J. Zeuner *et al.*, *"Integrated-optics heralded controlled-NOT gate for polarization-encoded qubits"*, npj Quantum Informationvolume **4**, 13 (2018)

[17] M. A. Nielsen and I. L. Chuang, *"Quantum Computation and Quantum Information"*, Cambridge Series on Information and the Natural Sciences (Cambridge Univ. Press, 2000)

[18] X. Qiang *et al.*, *"Large-scale silicon quantum photonics implementing arbitrary two-qubit processing"*, Nat. Photon. **12**, 534-539 (2018)

[19] X. Y. Zou, L. J. Wang, & L. Mandel, *"Induced coherence and indistinguishability in optical interference."*, Phys. Rev. Lett. **67**, 318–321 (1991).

[20] T. J. Herzog, P. G. Kwiat, H. Weinfurter, A. Zeilinger, W. Huang, *"Complementarity and the Quantum Eraser"*, Phys. Rev. Lett. **75**, 3034–632 (1995).

[21] A. Heuer, R. Menzel, and P. W. Milonni, *"Induced Coherence, Vacuum Fields, and Complementarity in Biphoton Generation"*, Phys. Rev. Lett. **114**, 053601 (2015).

[22] A. Heuer, R. Menzel, and P. W. Milonni, *"Complementarity in biphoton generation with stimulated or induced coherence"*, Phys. Rev. A **92**, 033834 (2015).

[23] J. Jing, C. Liu, Z. Zhou, Z. Y. Ou, & W. Zhang, *"Realization of a nonlinear interferometer with parametric amplifiers"*, Appl. Phys. Lett. **99**, 011110 (2011)

[24] Z. Y. Ou, *"Enhancement of the phase-measurement sensitivity beyond the standard quantum limit by a nonlinear interferometer"*, Phys. Rev. A **85**, 023815 (2012)

[25] B. Yurke, S. L. McCall, and J. R. Klauder, *"SU(2) and SU(1,1) interferometers"*, Phys. Rev. A **33**, 4033 (1986)

[26] F. Hudelist, J. Kong, C. Liu, J. Jing, Z. Y. Ou and W. Zhang, *"Quantum metrology with parametric amplifier-based photon correlation interferometers"*, Nat. Communs. **5**, 3049 (2014)

[27] T. J. Herzog, J. G. Rarity, H. Weinfurter and A. Zeilinger, *"Frustrated Two-Photon Creation via Interference"*, Phys. Rev. Lett. **72**, 629 (1994).

[28] G. B. Lemos *et al.*, *"Quantum imaging with undetected photons"*, Nature (London) **512**, 409 (2014).

[29] D. A. Kalashnikov, A. V. Paterova, S. P. Kulik & L. A. Krivitsky, *"Infrared spectroscopy with visible light"*, Nat. Photon. **10**, 98-101 (2016)

[30] M. Krenn, A. Hochrainer, M. Lahiri, and A. Zeilinger, *"Entanglement by Path Identity"*, Phys. Rev. Lett. **118**, 080401 (2017).

[31] R. Z. Vered, Y. Shaked, Y. Ben Or, M. Rosenbluh & A. Peer, *"Classical-to-Quantum Transition with Broadband Four-Wave Mixing"*, Phys. Rev. Lett. **114**, 063902-632 (2015).

[32] Q. Xu and M. Lipson, *"Carrier-induced optical bistability in silicon ring resonators"*, Opt. Lett. **31**, 341-343 (2006).